

Random sequential adsorption on partially covered surfaces

Zbigniew Adamczyk^{a)} and Paweł Weroński

Institute of Catalysis and Surface Chemistry, Polish Academy of Sciences, 30-239 Cracow, ul. Niezapominajek 1, Poland

(Received 24 October 1997; accepted 11 March 1998)

The random sequential adsorption (RSA) approach was used to analyze adsorption of hard spheres at surfaces precovered with smaller sized particles. Numerical simulations were performed to determine the available surface fraction ϕ_l of larger particles for various particle size ratios $\lambda = a_l/a_s$ and surface concentration of smaller particles θ_s . It was found that the numerical results were in a reasonable agreement with the formula stemming from the scaled particle theory with the modification for the sphere/sphere geometry. Particle adsorption kinetics was also determined in terms of the RSA simulations. By extrapolating the θ_l vs $\tau^{-1/2}$ dependencies, the jamming concentrations of larger spheres θ_l^∞ were determined as a function of the initial smaller sphere concentration. It was found that θ_l^∞ were considerably reduced by the presence of smaller sized particles, especially for $\lambda \gg 1$. The pair correlation function g of larger particles in the jamming state was also determined, showing more short range ordering (at the same θ_l) in comparison with monodisperse systems. The theoretical predictions stemming from our calculations suggest that the presence of trace amounts of very small particles may exert a decisive influence on adsorption of larger particles. © 1998 American Institute of Physics. [S0021-9606(98)50923-3]

INTRODUCTION

The random sequential adsorption (RSA) is one of the simplest and most efficient approaches to analyze sequences of irreversible events. In this process objects (particles) of various geometrical shape are added randomly, one at a time, to a D -dimensional volume. Once an empty space element is found the particle is permanently fixed (with no consecutive motion allowed). Otherwise it is rejected and a new addition attempt is undertaken, uncorrelated with previous attempts. The process usually starts from an empty volume and continues until the jamming state is reached when no additional object (of the same size and shape) can be added. Exact solutions of the RSA problem exist for one-dimensional problems only.^{1,2} For higher dimensionality abundant numerical studies exist³⁻⁹ in which kinetics of the RSA processes and jamming concentrations were determined in *ab initio*-type calculations. These results obtained for monodisperse spherical particles proved useful for interpreting irreversible adsorption phenomena of macromolecules, proteins, and colloid particles.^{10,11}

However, for a broad range of practical situations this classical RSA model seems inadequate, especially for processes when polydisperse suspensions or mixtures are occurring, e.g., colloid/polymer, colloid/colloid, or protein/surfactant. Due to their higher diffusivity and concentration, the smaller sized particles will first adsorb at the interface, forming a layer which may exert a significant influence on consecutive adsorption of larger particles. Similar problems may appear in model experiments concerning colloid particle or protein adsorption when the usual cleaning procedure may

produce a layer of contamination at the substrate surface difficult to detect. This is expected to affect adsorption kinetics in the proper experiments. Hence, the subject of particle adsorption at partially covered surfaces seems attractive from a practical viewpoint.

The studies on RSA processes at covered surfaces, are also attractive theoretically in view of the limited literature on this subject. The existing works were concerned with the related problem of polydisperse disk adsorption, which is strictly two dimensional. Talbot and Schaafl¹² performed an approximate analysis of adsorption of two-component (bimodal) mixtures of disks widely differing in diameter. Adsorption kinetics and the jamming concentrations of larger disks were determined in the limit when the size of the smaller disk decreased to zero. In the case of spheres they were unable to find the proper jamming limit.

Meakin and Jullien¹³ performed extensive simulations of adsorption kinetics and jamming limit for polydisperse disk mixtures characterized by bimodal, uniform, and truncated Gaussian distributions.

The quasi-three-dimensional problem of polydisperse sphere adsorption was treated in Ref. 14. However, the numerical simulations performed for hard and soft spheres according to the RSA model, were confined to suspensions characterized by narrow size distributions, i.e., 0%–20% only.

In this paper we report numerical simulations concerning adsorption of larger spheres at surfaces precovered with significantly smaller spheres. Adsorption kinetics, jamming coverages, and radial distribution function of large particles will be determined.

The problem considered in our work can be treated as the extension of the classical RSA to systems characterized

^{a)} Author to whom correspondence should be addressed. Electronic mail: ncadamcz@cyf.-kr.edu.pl

by a discontinuous change (increase) of the size of the objects added to a volume.

It should be mentioned that some preliminary results on adsorption kinetics at covered surfaces have been published in Ref. 15.

THE SIMULATION METHOD

The simulation algorithm was similar to that used for polydisperse sphere adsorption described in Ref. 14. The simulations were carried out over a rectangular simulation plane with the usual periodic boundary conditions at its perimeter. As in previous works,^{6-8,13} the simulation plane was divided into subsidiary square areas (cells) of the size $\sqrt{2}a_s$ (where a_s is the radius of the smaller particle) so the center of at most one particle could lie within a particular cell. This enhanced the efficiency of the overlapping test performed at each simulation step.

The entire simulation procedure consisted of two main stages:

- (i) the simulation plane was covered with smaller sized particles to a prescribed dimensionless surface concentration (coverage) $\theta_s = \pi a_s^2 N_s$ (where N_s is the surface density of smaller spheres), during this stage the usual RSA simulation algorithm was used;
- (ii) then the larger spheres, having the radius a_l were introduced by choosing at random their position within the simulation area; the overlapping test between larger/larger and smaller/larger particles was carried out in the latter case by considering the true three-dimensional distances between the sphere centers.

In order to simulate the kinetic runs the dimensionless adsorption time τ was set to zero at the beginning of the second stage. In calculations τ was defined as

$$\tau = \frac{N_{\text{att}}}{N_{\text{ch}}} = \pi \bar{a}_l^2 N_{\text{att}}, \quad (1)$$

where $N_{\text{ch}} = (1/\pi \bar{a}_l^2)$ is the characteristic surface concentration of larger particles and N_{att} is the overall number of attempts to place larger particles.

The maximum dimensionless time attained in our simulation was about 10^4 which required 10^6 – 10^9 simulation steps. The jamming concentrations θ^∞ were calculated by extrapolating the results obtained for this limiting dimensionless time, assuming power law dependencies. In order to attain a sufficient accuracy, averages from many computer runs were taken.

The available surface function (ASF) for larger particles ϕ_1 was calculated according to the method of Schaaf and Talbot⁴ by exploiting the definition

$$\phi_1 = \frac{p(\theta_s, \theta_l)}{p_0} = \frac{N_{\text{succ}}}{N_{\text{att}}}, \quad (2)$$

where p is the probability of adsorbing the larger particle at the surface characterized by the coverages θ_s , θ_l , p_0 is the probability of adsorption at uncovered surface (assumed equal one without loss of generality) and N_{succ} is the number

of successful adsorption events performed at fixed θ_s , θ_l . In practice, N_{att} was about 10^5 in order to attain a sufficient accuracy of ϕ_1 .

The pair correlation function (radial distribution function) g was determined using the definition, i.e., from the equation

$$g(\mathbf{r}) = \frac{S}{N^2} \left\langle \sum_{i=1}^N \sum_{j=1}^N \delta_D[\mathbf{r} - (\mathbf{r}_j - \mathbf{r}_i)] \right\rangle, \quad (3)$$

where \mathbf{r} is the position vector of a point over the adsorption plane (measured from the center of an adsorbed particle), S is the surface area for which the g function should be evaluated, N is total number of particles adsorbed over this area, δ_D is the Dirac delta function, $\mathbf{r}_i, \mathbf{r}_j$ are the position vectors of the i and j particle, and angle brackets means the ensemble average.

In absence of external forces when the system can be treated as isotropic, the vector \mathbf{r} can be replaced by the radial coordinate r and the pair correlation function can be calculated more directly by converting Eq. (3) to the form

$$g(\mathbf{r}) = g(r) = \frac{S}{N} \frac{\bar{N}_a(r)}{2\pi r \Delta r}, \quad (4)$$

where $\bar{N}_a(r) = (1/N) \langle N_a \rangle$ is the averaged number of particles within the annulus of the mean radius r and the thickness Δr .

For evaluating g the coordinates of about 20 000 particles were considered.

All calculations discussed hereafter were performed for particle size ratio $\lambda = a_l/a_s$ of 2.2 (this was chosen to match the experimental conditions), 5 and 10.

ANALYTICAL APPROXIMATION

Due to a lack of appropriate expressions for the available surface function in the case of RSA of large particles at precovered surfaces, we tested our results in terms of the equilibrium adsorption approaches. This seems reasonable since θ_l at precovered surfaces is generally much smaller than for uncovered surfaces.

According to the scaling particle theory (SPT) formulated in Ref. 16 and then extended to multicomponent mixtures in Refs. 17 and 18, the equilibrium ASF functions for bimodal suspension of disks of radius a_1 and a_2 are given by the expressions

$$\phi_1 = -\ln \left(\frac{\mu_1^R}{kT} \right) = (1-\theta) \exp \left[-\frac{3\theta_1 + (1/\gamma)(1/\gamma+2)\theta_2}{1-\theta} - \left(\frac{\theta_1 + (1/\gamma)\theta_2}{1-\theta} \right)^2 \right], \quad (5)$$

$$\phi_2 = -\ln \left(\frac{\mu_2^R}{kT} \right) = (1-\theta) \exp \left[-\frac{3\theta_2 + \gamma(\gamma+2)\theta_1}{1-\theta} - \left(\frac{\theta_2 + \gamma\theta_1}{1-\theta} \right)^2 \right],$$

where μ_1^R and μ_2^R are the residual potentials of the smaller and larger particles, respectively, $\theta = \theta_1 + \theta_2$ and $\gamma = a_2/a_1$ is the disk size ratio. It should be noted that Eq. (5) describes a two-dimensional situation only.

It seems, however, that useful approximations of the sphere adsorption problem (a quasi-three-dimensional situation) can be formulated by redefining the geometrical parameter γ . Thus, by expanding Eq. (5) in the power series of θ (up to the order of two) one obtains the expression

$$\begin{aligned} \phi_1 &\cong 1 - 4\theta_1 - (1/\gamma + 1)^2\theta_2 + 0(\theta_1\theta_2, \theta_1^2, \theta_2^2), \\ \phi_2 &\cong 1 - 4\theta_2 - (\gamma + 1)^2\theta_1 + 0(\theta_1\theta_2, \theta_1^2, \theta_2^2). \end{aligned} \tag{6}$$

Now, from the general result of Widom¹⁹ it can be deduced that

$$\phi_1 \cong 1 - \bar{S}_1\theta_1 - \frac{\bar{S}_{12}}{\lambda^2}\theta_2 + 0(\theta_1\theta_2, \theta_1^2, \theta_2^2), \tag{7}$$

$$\phi_2 \cong 1 - \bar{S}_1\theta_2 - \bar{S}_{12}\theta_1 + 0(\theta_1\theta_2, \theta_1^2, \theta_2^2),$$

where $\pi a_1^2 \bar{S}_1$, $\pi a_2^2 \bar{S}_{12}$, are the exclusion areas for two smaller spheres and for the smaller/larger sphere, respectively.

From the elementary geometry one has

$$\begin{aligned} \bar{S}_1 &= 4, \\ \bar{S}_{12} &= 4\lambda. \end{aligned} \tag{8}$$

Thus, Eq. (7) can be matched with the series expansion Eq. (6) when

$$\gamma = 2\sqrt{\lambda} - 1. \tag{9}$$

Denoting $a_1 = a_s$ and $a_2 = a_l$ and using Eqs. (9) and (5) one can derive the analytical expression for the ASF function of larger particles at surfaces precovered with smaller particles in the form

$$\begin{aligned} \phi_l(\theta_s, \theta_l) &= (1 - \theta) \exp \left\{ - \frac{3\theta_l + (4\lambda - 1)\theta_s}{1 - \theta} \right. \\ &\quad \left. - \left[\frac{\theta_l + (2\sqrt{\lambda} - 1)\theta_s}{1 - \theta} \right]^2 \right\} \\ &= \phi_l^0(\theta_s) \left(1 - \frac{\theta_l}{1 - \theta_s} \right) \exp \left\{ - \frac{4(\lambda - 1)\theta_s + 3}{1 - \theta_s} \frac{\theta_l}{1 - \theta} \right. \\ &\quad \left. - \left[\theta_l - \frac{(2\sqrt{\lambda} - 1)^2 \theta_s^2 \theta_l}{(1 - \theta_s)^2} + \frac{2(2\sqrt{\lambda} - 1)^2 \theta_s^2}{1 - \theta_s} \right. \right. \\ &\quad \left. \left. + 2(2\sqrt{\lambda} - 1)\theta_s \right] \frac{\theta_l}{(1 - \theta)^2} \right\}, \end{aligned} \tag{10}$$

where $\theta = \theta_s + \theta_l$ and

$$\begin{aligned} \phi_l^0(\theta_s) = \bar{j}_0 &= (1 - \theta_s) \exp \left\{ - \frac{(4\lambda - 1)\theta_s}{1 - \theta_s} \right. \\ &\quad \left. - \left[\frac{(2\sqrt{\lambda} - 1)\theta_s}{1 - \theta_s} \right]^2 \right\} \end{aligned} \tag{11}$$

is the ASF function of larger particles for $\theta_l = 0$ and \bar{j}_0 can be treated as the dimensionless adsorption flux of larger particles at surfaces precovered with smaller particles.

The low coverage expansion of Eq. (10) up to the second order of θ_l is

$$\frac{\phi_l}{\phi_l^0} = 1 - C'_1(\theta_s)\theta_l + C'_2(\theta_s)\theta_l^2 + 0(\theta_l^3), \tag{12}$$

where the constants C'_1 and C'_2 are

$$\begin{aligned} C'_1 &= \frac{4 + (4\lambda + 4\sqrt{\lambda} - 7)\theta_s + 2(2\sqrt{\lambda} - 1)^2 \theta_s^2 / (1 - \theta_s)}{(1 - \theta_s)^2}, \\ C'_2 &= \frac{a(\theta_s)}{(1 - \theta_s)^3} + \frac{a^2(\theta_s)}{2(1 - \theta_s)^4} + \frac{b(\theta_s)}{(1 - \theta_s)^2}, \end{aligned} \tag{13}$$

$$a(\theta_s) = 3 + 2(2\lambda + 2\sqrt{\lambda} - 3)\theta_s + 2(2\sqrt{\lambda} - 1)^2 \frac{\theta_s^2}{1 - \theta_s},$$

$$b(\theta_s) = - \left[4 + \theta_s \frac{4\lambda + 8\sqrt{\lambda} - 5}{1 - \theta_s} + 3 \left(\frac{(2\sqrt{\lambda} - 1)\theta_s}{1 - \theta_s} \right)^2 \right].$$

By neglecting the θ_l^2 term one can formally convert Eq. (12) to the quasi-Langmuirian form, i.e.,

$$\frac{\phi_l}{\phi_l^0} = 1 - \frac{\theta_l}{\theta_{\text{mx}}}, \tag{14}$$

where

$$\theta_{\text{mx}} \cong \frac{1}{4 + (4\lambda + 4\sqrt{\lambda} - 7)\theta_s}. \tag{15}$$

The advantage of this formulation over the semiempirical Langmuir model widely used in the literature is that θ_{mx} values can be calculated *a priori* for a given coverage of smaller particles.

RESULTS AND DISCUSSION

Using the above RSA algorithm extensive calculations were performed for determining both the ASF functions of larger particles, their adsorption kinetics, jamming coverages, and the structure of adsorbed layer.

The quantity of considerable practical interest is the $\phi_l^0(\theta_s)$ function which represents the averaged probability of adsorbing larger particle over a surface precovered by smaller particles (characterized by the coverage θ_s) normalized to the probability of adsorbing the particle over an uncovered surface. In Fig. 1 the dependence of ϕ_l^0 on θ_s is plotted for $\lambda = 1$ (reference curve for monodisperse spheres), 2.2, 5, and 10, respectively. As can be noticed, adsorption probability of larger particles is considerably decreased by the presence of adsorbed small particles, especially for higher λ values. Note that the available experimental data¹⁵ seem to be in a good agreement with the RSA simulations for $\lambda = 2.2$.

It is also interesting to observe that the analytical SPT results represented by Eq. (11) reflect well the characteristic features of the ϕ_l^0 function. The agreement between the RSA simulations and these analytical predictions seems quantitative when $\phi_l^0 > 0.1$. As expected the deviation between equi-

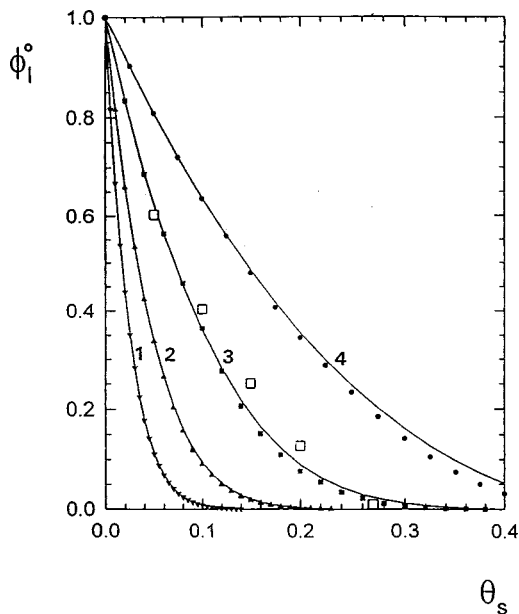


FIG. 1. The dependence of ϕ_1^0 on surface concentration of smaller particles θ_s . The points denote numerical simulations performed for: (1) $\lambda=10$, (2) $\lambda=5$, (3) $\lambda=2.2$, (4) $\lambda=1$ (reference, monodisperse system). The continuous lines denote the equilibrium SPT results calculated from Eq. (11) and empty squares represent the experimental results obtained for bimodal suspension of polymeric colloid particles Ref. 15.

librium and RSA results increased for higher θ_s values when ϕ_1^0 became considerably smaller than 0.1. One may, therefore, conclude that the presence of trace amounts of smaller (e.g., colloid type) particles, hardly detectable by conventional means, should exert a profound effect on adsorption of larger particles (cf. curve 1 in Fig. 1 obtained for $\lambda=10$).

The result shown in Fig. 1 suggest also that the SPT results can be used for practical purposes as a good estimate of ϕ_1^0 (initial flux) on precovered surfaces.

Similar, although considerably more time-consuming calculations were performed to determine the dependence of the ϕ_1 function on the concentration of larger particles θ_l for fixed θ_s values. The results obtained for $\lambda=2.2$ are plotted in Fig. 2. One can observe that the presence of smaller particles considerably reduces ϕ_1 which can be well described by the analytical predictions stemming from Eq. (10). However, some positive deviations of the SPT results from the RSA appeared for $\theta_s > 0.2$. Since the ϕ_1 function assumes small values for this range of θ_s the differences are difficult to observe. Analogous calculations performed for $\lambda=10$ are plotted in Fig. 3.

As can be seen in Figs. 2–3, the deviations of the SPT results from the RSA calculations become quite significant for higher θ_s , especially for $\lambda=10$. However, for smaller θ_s the SPT results can be accepted as a reasonable estimate of ϕ_1 .

By knowing the ASF function one can determine the irreversible adsorption kinetics of larger particles from the defining integral

$$\theta_l = k_a c_l S_g \int \phi_1 dt = \int \phi_1 d\tau, \quad (16)$$

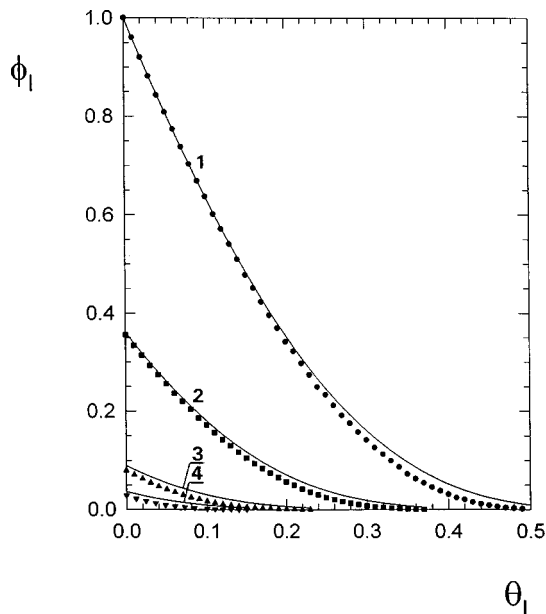


FIG. 2. The dependence of the ϕ_1 function of larger particles on θ_l calculated numerically for $\lambda=2.2$ and (1) $\theta_s=0$, (2) $\theta_s=0.10$, (3) $\theta_s=0.20$, (4) $\theta_s=0.25$. The continuous lines denote the equilibrium SPT results calculated from Eq. (10).

where $k_a = j_0/c_l$ is the adsorption constant, c_l is the bulk concentration of larger particles, S_g is the characteristic area (usually the particle cross-section area), t is the dimensional adsorption time and $\tau = k_a c_l S_g t$ is the dimensionless adsorption time.

As demonstrated previously¹¹ this dimensionless time corresponds to that used in numerical simulations defined by Eq. (1).

Equation (16) can be used when ϕ_1 is known analytically, e.g., for the SPT or quasi-Langmuir model. In the latter

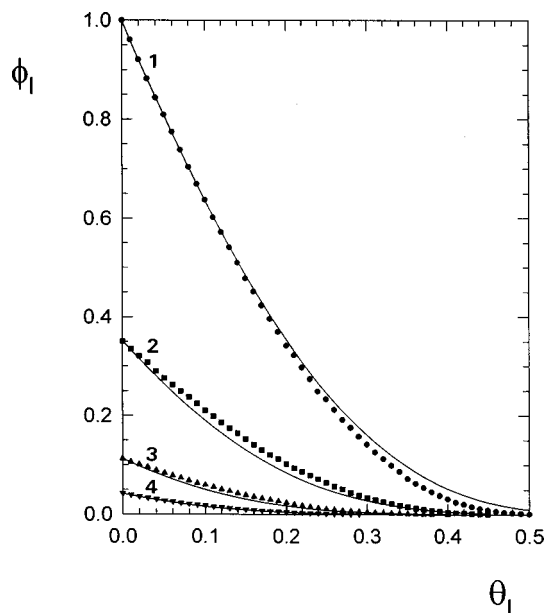


FIG. 3. Same as for Fig. 2 but for $\lambda=10$. (1) $\theta_s=0$, (2) $\theta_s=0.025$, (3) $\theta_s=0.050$, (4) $\theta_s=0.070$. The continuous lines denote the equilibrium SPT results calculated from Eq. (10).

case the integral can be evaluated explicitly giving the simple expression

$$\theta_l = \theta_{mx} \left[1 - \exp\left(-\frac{\phi_l^0}{\theta_{mx}} \tau\right) \right] \quad (17)$$

with θ_{mx} defined by Eq. (15) and ϕ_l^0 by Eq. (11).

In the case when ϕ_l is known numerically the use of Eq. (16) is less efficient in comparison with direct numerical simulations of adsorption kinetics according to the algorithm described above.

In Figs. 4 the kinetic curves, i.e., the θ_l vs τ dependencies, are plotted for $\lambda=2.2$ and $\lambda=10$ (part ‘‘b’’) derived from the numerical simulations for various surface concentration θ_s . The analytical results calculated from the quasi-Langmuirian model, i.e., Eq. (17) are also shown for comparison. As can be seen the quasi-Langmuirian model can be used as a reasonable estimate of adsorption kinetics on precovered surfaces for adsorption times $\tau < 1$ (the range of validity of this model seems to increase with θ_s). For longer times one can observe, however, systematic deviations of the simulated θ_l values from the apparent saturation coverages θ_{mx} .

In order to compress the infinite time domain into a finite one $\tau^{-1/2}$ was used as the independent variable for $\tau > 4$ (right-hand side of Figs. 4). This transformation was successfully applied previously³⁻⁵ for presenting the RSA results for uncovered surfaces when

$$\theta_\infty - \theta_l \sim \tau^{-1/2}, \quad (18)$$

where θ_∞ is the jamming coverage for monodisperse spheres calculated to be 0.547.⁹

Thus when plotting θ_l vs $\tau^{-1/2}$, a straight line dependence should be obtained. As can be observed in Figs. 4 this seems to be the case for adsorption at precovered surfaces. However, the range of the asymptotic regime characterized by the power-law dependence of θ_l on τ was decreased considerably with the increase in θ_s .

The occurrence of these asymptotic regimes implies, therefore, that for longer adsorption times isolated targets existed only whose size distribution was uniform.³

One can also deduce that the θ_l vs $\tau^{-1/2}$ dependence implies that the ASF function for the asymptotic regime should assume the form

$$\phi_l \sim [\theta_l^\infty(\theta_s) - \theta_l]^3, \quad (19)$$

where the jamming coverages θ_l^∞ are dependent on the initial coverage of smaller particles.

In our calculations these jamming concentrations were obtained by the linear fitting of the θ_l vs $\tau^{-1/2}$ dependencies and subsequent extrapolation to $\tau^{-1/2} = 0$ ($\tau \rightarrow \infty$). Averages from five independent computer runs were taken in order to attain a sufficient precision of θ_l^∞ . These data are compiled in Table I for $\lambda = 2.2, 5,$ and 10 .

The dependencies of the jamming concentrations θ_l^∞ on θ_s are also shown graphically in Fig. 5. For sake of convenience the total coverage, i.e., the sum $\theta_s + \theta_l^\infty$ is also plotted in Fig. 5. The characteristic feature of the θ_l^∞ vs θ_s dependencies is that they fall abruptly to very small values when θ_s is increased.

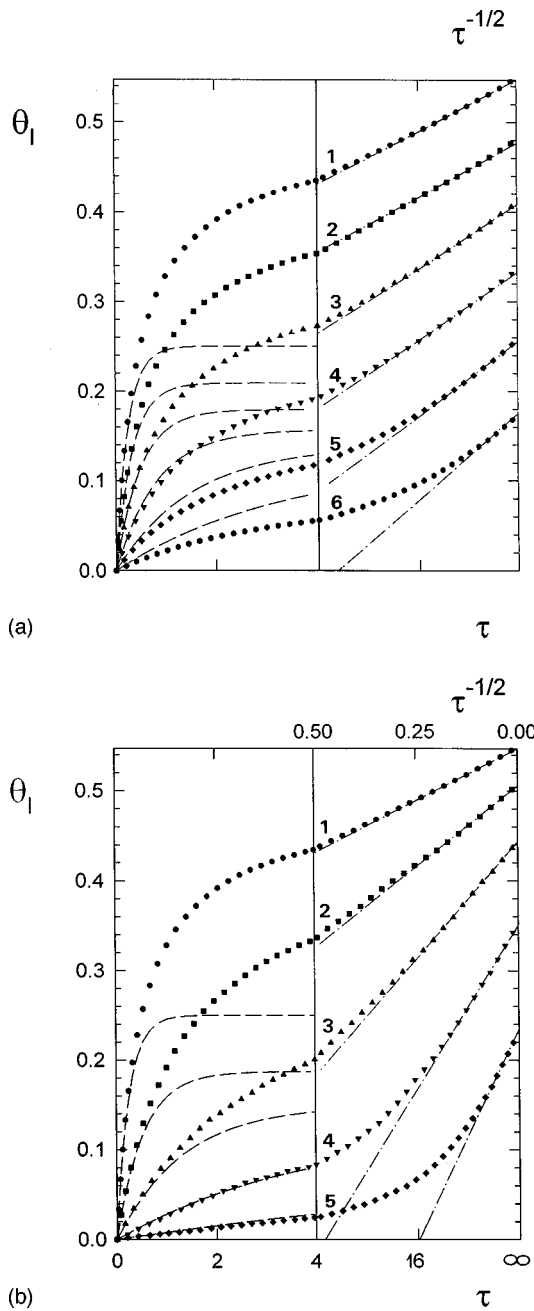


FIG. 4. Kinetics of larger particle adsorption at surfaces precovered with smaller particles expressed as θ_l vs τ dependencies; (a) $\lambda = 2.2$ (1) $\theta_s = 0$, (2) $\theta_s = 0.05$, (3) $\theta_s = 0.10$, (4) $\theta_s = 0.15$, (5) $\theta_s = 0.20$, (6) $\theta_s = 0.25$. The broken lines denote the analytical results calculated from Eq. (17) and the -.-. lines denote the linear fits, i.e., $\theta_l^\infty - \theta_l \sim \tau^{-1/2}$. (b) same as for (a) but for $\lambda = 10$ and (1) $\theta_s = 0$, (2) $\theta_s = 0.025$, (3) $\theta_s = 0.05$, (4) $\theta_s = 0.07$, (5) $\theta_s = 0.10$.

It has been found that the numerical results can well be fitted by the interpolating functions (cf. solid lines in Fig. 5)

$$\theta_l^\infty = \theta_\infty^{[c/(c-\theta_s)]^2}, \quad (20)$$

where c are the dimensionless constants equal 0.596 for $\lambda = 2.2$; 0.404 for $\lambda = 5$ and 0.274 for $\lambda = 10$.

On the other hand, in the low coverage limit, i.e., for $\theta_l^\infty < 0.1$ the character of the numerical data can better be reflected by the interpolating function

TABLE I. Jamming concentration of larger spheres θ_l^∞ at precovered surfaces.

θ_s	θ_l^∞	$\theta_l^\infty + \theta_s$
$a_l/a_s=2.2$		
0.0000	0.5470	0.5470
0.0500	0.4762±0.0026	0.5262
0.1000	0.4079±0.0022	0.5079
0.1500	0.3326±0.0033	0.4826
0.2000	0.2550±0.0054	0.4550
0.2500	0.1750±0.0020	0.4250
0.3000	0.0900±0.0030	0.3900
0.3200	0.0604±0.0008	0.3804
0.3400	0.0378±0.0017	0.3778
0.3600	0.0193±0.0017	0.3793
0.3800	0.0080±0.0010	0.3880
0.4000	0.0024±0.0007	0.4025
$a_l/a_s=5$		
0.0000	0.5470	0.5470
0.0500	0.4735±0.00018	0.5235
0.1000	0.3680±0.0009	0.4680
0.1500	0.2249±0.0015	0.3749
0.1700	0.1640±0.0020	0.3340
0.2000	0.0832±0.0023	0.2832
0.2200	0.0455±0.0011	0.2655
0.2400	0.0206±0.0008	0.2606
0.2500	0.0137±0.0012	0.2637
0.2600	0.0082±0.0007	0.2682
0.2700	0.0049±0.0005	0.2749
$a_l/a_s=10$		
0.0000	0.5470±0.0021	0.5470
0.0200	0.5134±0.0021	0.5334
0.0400	0.4704±0.0021	0.5104
0.0600	0.4080±0.0020	0.4680
0.0800	0.3302±0.0016	0.4102
0.0900	0.2830±0.0017	0.3730
0.1000	0.2341±0.0024	0.3341
0.1100	0.1800±0.0030	0.2900
0.1200	0.1350±0.0040	0.2550
0.1300	0.0944±0.0009	0.2244
0.1400	0.0620±0.0050	0.2020
0.1500	0.0384±0.0021	0.1884
0.1600	0.0208±0.0004	0.1808
0.1700	0.0110±0.0010	0.1810
0.1800	0.0060±0.0010	0.1860

$$\theta_l^\infty = c\lambda \phi_l^0(\theta_s), \quad (21)$$

where $\phi_l^\infty(\theta_s)$ is the ASF function given by Eq. (11) and c are the dimensionless constants equal explicitly 3.78 for $\lambda = 2.2$; 6.67 for $\lambda = 5$ and 9.3 for $\lambda = 10$. Another interesting feature of the data shown in Fig. 5 is that the net surface coverage of adsorbed particles passes through a minimum whose depth increased considerably for larger λ . The minimum coverages were found to be 0.378 for $\lambda = 2.2$ ($\theta_s = 0.34$) 0.261 for $\lambda = 5$ ($\theta_s = 0.24$) and 0.181 for $\lambda = 10$ ($\theta_s = 0.16$). These results represent a spectacular manifestation of the irreversibility effect since the composition and density of ‘‘monolayers’’ formed by particles is dependent on the peculiarities of the adsorption path, e.g., order of bringing particles to the interface. Physically, this can be realized by replacing the smaller particle suspension after a given adsorption time by the larger particle suspension.

This effect is also demonstrated in Figs. 6(a)–6(c) where various monolayers under the jamming state are shown (simulated numerically for $\lambda = 2.2$ and $\tau = 10^4$). Depending

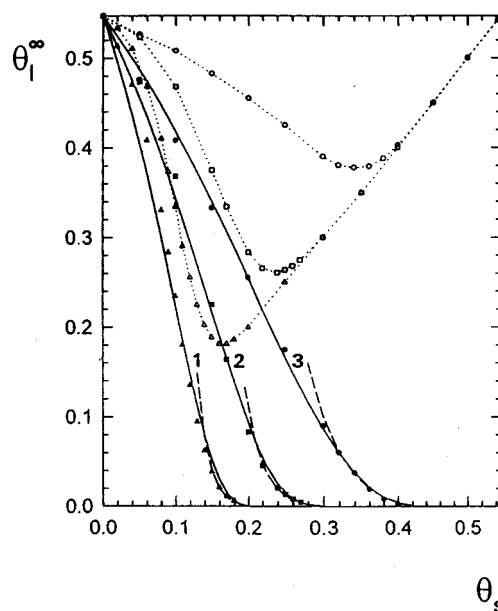


FIG. 5. The dependence of the jamming concentration of larger particles θ_l^∞ on surface concentration of smaller particles θ_s ; the points (full symbols) denote results of numerical simulations performed for (1) $\lambda = 10$, (2) $\lambda = 5$, (3) $\lambda = 2.2$. The empty symbols represent the net coverage, i.e., $\theta_l^\infty + \theta_s$, the continuous lines represent the fitting functions given by Eq. (20) and the broken lines show the limiting results calculated from Eq. (21).

on the initial value of θ_s , a complete jamming was attained for the total coverage ranging between 0.39 [Fig. 6(a)] and 0.51 [Fig. 6(c)].

The distributions of larger particles shown in Figs. 6 seem also qualitatively different from analogous distributions (at the same coverage) observed previously for monodisperse systems.¹¹ This was demonstrated quantitatively by determining the radial distribution function of larger particles g_l according to the method described above. The results are shown in Figs. 7(a)–7(c) for θ_l equal 0.09, 0.25 and 0.41, respectively. For comparison the g_l function determined from numerical simulations for a monodisperse system at the same surface coverage is also plotted in Figs. 7. As can be seen, for the bimodal system at low coverages, the shape of the radial distribution function deviates significantly from its monodisperse counterpart, especially for low coverages θ_l . Thus for $\theta_l = 0.09$ of Fig. 7(a) a well-pronounced depletion zone can be observed (for $2 < r/a_l < 2.6$) followed by a maximum of a considerable height. By contrast, for monodisperse system the g_l function decreased monotonically for this range of distances. It is interesting to note that the shape of the g_l function for bimodal systems is quite analogous to the radial distribution functions predicted theoretically and observed experimentally for monodisperse systems of electrostatically interacting particles.¹¹

However, in the case of bimodal systems the depletion zone effect is caused by the fact that larger particle adsorption occurs mostly at isolated targets separated from each other by distances comparable with the smaller particle diameter.

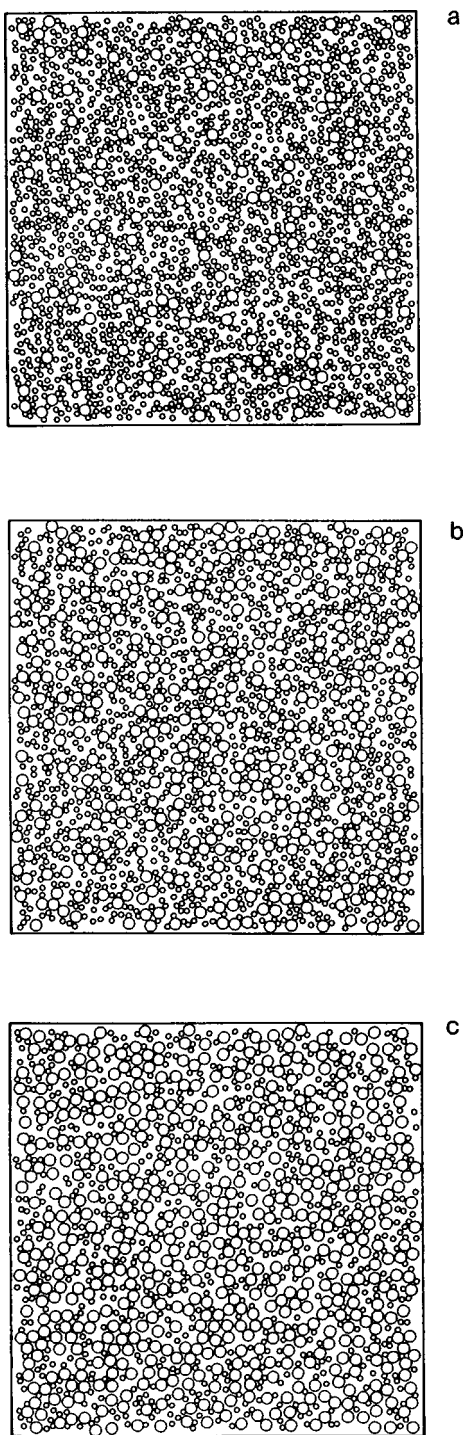


FIG. 6. The adsorbed particle "monolayers" close to the jamming limit simulated numerically for $\lambda=2.2$. (a) $\theta_s=0.3$, $\theta_l=0.09$. (b) $\theta_s=0.2$, $\theta_l=0.25$. (c) $\theta_s=0.1$, $\theta_l=0.41$.

The results shown in Figs. 7 suggest that from the shape of the g_l function of larger particles important information can be extracted concerning the concentration and the size of preadsorbed particles.

CONCLUDING REMARKS

It was found that the numerical RSA simulations concerning adsorption at precovered surfaces can well be approximated in the limit of low densities by the extrapolated

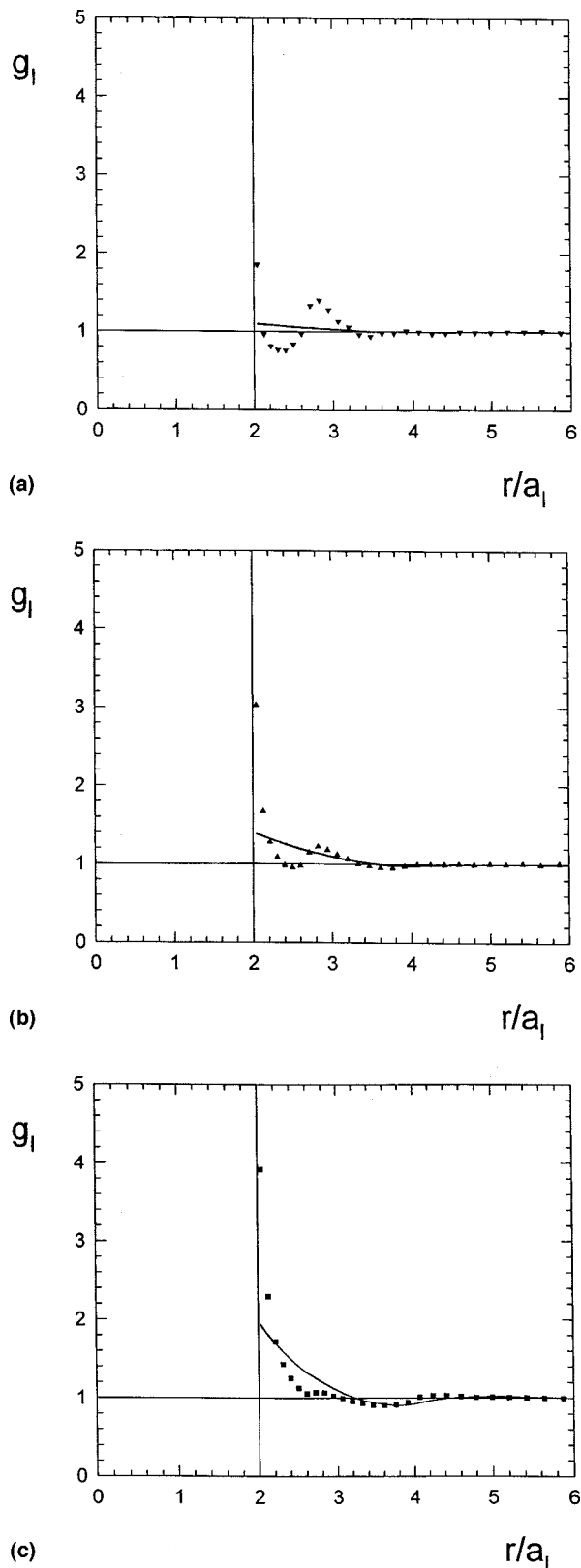


FIG. 7. The pair correlation function of larger particles g_l derived from numerical simulations for $\lambda=2.2$. (a) $\theta_s=0.3$, $\theta_l=0.09$. (b) $\theta_s=0.2$, $\theta_l=0.25$. (c) $\theta_s=0.1$, $\theta_l=0.41$. The continuous lines denotes the smoothed results obtained for monodisperse systems characterized by the same θ_l .

SPT theory with the geometrical parameter $\gamma=2\sqrt{a_l/a_s}-1$ instead of a_l/a_s for disks (2D case). As a direct manifestation of irreversibility it was also shown that the total jamming coverage of bimodal mixtures passes through a mini-

mum whose depth may become considerable for larger λ values. These theoretical predictions derived from the RSA simulations suggest that both the adsorption kinetic (initial flux) and the jamming coverages of particles are very sensitive to the presence at interfaces of trace amounts of smaller sized particles often difficult to detect by conventional analytical means. These theoretical prediction may explain the persisting difficulties in obtaining reliable kinetic data and monolayer densities in protein adsorption processes being usually of an irreversible character.

In comparison with monodisperse systems, adsorption at precovered surfaces is leading to different structures, characterized in terms of the radial distribution function. Hence, by determining g_l for larger particles important clues about the presence of smaller sized preadsorbed particles (contaminants) can be drawn.

ACKNOWLEDGMENT

This work was partially supported by the KBN Grant No. 3T09 A08310.

- ¹A. Renyi, Publ. Math. Inst. Hung. Acad. Sci. **3**, 109 (1958).
- ²J. J. Gonzales, P. C. Hemmer, and J. S. Hoye, Chem. Phys. **3**, 288 (1974).
- ³E. L. Hinrichsen, J. Feder, and T. Jossang, J. Stat. Phys. **44**, 793 (1986).
- ⁴P. Schaaf and J. Talbot, J. Chem. Phys. **91**, 4401 (1989).
- ⁵J. Talbot, G. Tarjus, and P. Schaaf, Phys. Rev. A **4**, 4808 (1989).
- ⁶S. M. Ricci, J. Talbot, G. Tarjus, and P. Viot, J. Chem. Phys. **97**, 5219 (1992).
- ⁷J. Talbot, P. Schaaf, and G. Tarjus, Mol. Phys. **72**, 1397 (1991).
- ⁸Z. Adamczyk and P. Weroński, J. Chem. Phys. **105**, 5562 (1996).
- ⁹J. W. Evans, Rev. Mod. Phys. **65**, 1281 (1993).
- ¹⁰J. J. Ramsden, Phys. Rev. Lett. **71**, 295 (1993).
- ¹¹Z. Adamczyk, B. Siwek, M. Zembala, and P. Belouchek, Adv. Colloid Interface Sci. **48**, 151 (1994).
- ¹²J. Talbot, and P. Schaaf, Phys. Rev. A **40**, 422 (1989).
- ¹³P. Meakin, and R. Jullien, Phys. Rev. A **46**, 2029 (1991).
- ¹⁴Z. Adamczyk, B. Siwek, M. Zembala, and P. Weroński, J. Colloid Interface Sci. **185**, 236 (1997).
- ¹⁵Z. Adamczyk, B. Siwek, and P. Weroński, J. Colloid Interface Sci. **195**, 261 (1997).
- ¹⁶H. Reiss, H. L. Frisch, and J. L. Lebowitz, J. Chem. Phys. **31**, 369 (1959).
- ¹⁷J. L. Lebowitz, E. Helfand, and E. Praestgaard, J. Chem. Phys. **43**, 774 (1965).
- ¹⁸J. Talbot, X. Jin, and N. H. L. Wang, Langmuir **10**, 1663 (1994).
- ¹⁹B. Widom, J. Chem. Phys. **44**, 3888 (1966).